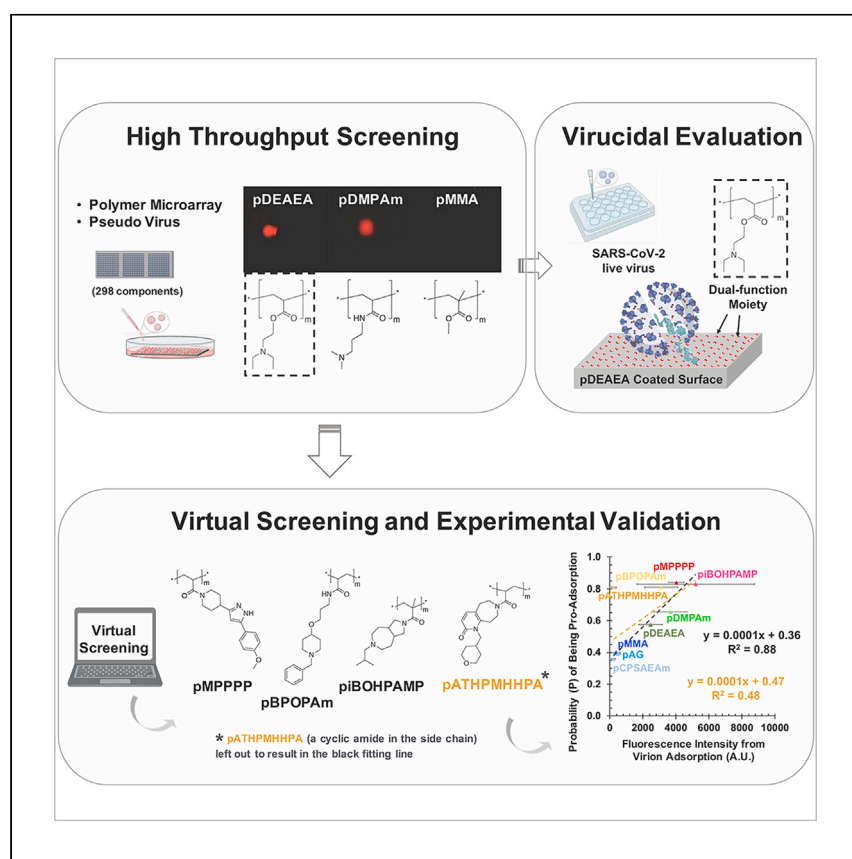


Article

Discovery and computational modeling of adsorbent polymers that effectively immobilize SARS-CoV-2, with potential practical applications



Simple polymers that immobilize severe acute respiratory syndrome coronavirus 2 (SARS-CoV-2) upon contact provide an opportunity to develop new coating materials for better infection control. Here, Xue et al. discovered strong virion-binding polymers and investigated the mechanisms of virion-surface interaction with the aid of virtual screening using monomeric molecular descriptors.

Xuan Xue, Joshua D. Duncan, Christopher M. Coleman, ..., Jonathan K. Ball, Cameron Alexander, Morgan R. Alexander

xuan.xue@xjtlu.edu.cn (X.X.)
morgan.alexander@nottingham.ac.uk (M.R.A.)

Highlights

SARS-CoV-2-binding polymers are discovered

Computational models are built for structure prediction and mechanism investigation

pDEAEA demonstrates dual functions against SARS-CoV-2



Article

Discovery and computational modeling of adsorbent polymers that effectively immobilize SARS-CoV-2, with potential practical applications

Xuan Xue,^{1,2,7,*} Joshua D. Duncan,^{3,4} Christopher M. Coleman,^{3,4} Leonardo Contreas,⁵ Chester Blackburn,¹ Maria Vivero-Lopez,¹ Philip M. Williams,⁵ Jonathan K. Ball,^{3,4,6} Cameron Alexander,⁵ and Morgan R. Alexander^{1,*}

SUMMARY

Viral translocation is considered a common way for respiratory viruses to spread and contaminate the surrounding environment. Thus, the discovery of non-eluting polymers that immobilize severe acute respiratory syndrome coronavirus 2 (SARS-CoV-2) upon contact provides an opportunity to develop new coating materials for better infection control. Here, virion-binding polymers are discovered from an existing monomer library via experimental high-throughput screening. Among them, poly([2-diethylamino] ethyl acrylate) (pDEAEA) demonstrates dual functions: binding virions strongly and its speed to inactivate adsorbed SARS-CoV-2. Computational models are built based on the experimental screening data. Polymers that are predicted to be pro-adsorption by the virtual screening are poly(1-{4-[5-(4-methoxyphenyl)-1H-pyrazol-3-yl]piperidin-1-yl}prop-2-en-1-one) (pMPPPP), poly(1-(6-isobutyloctahydropyrrolo[3,4-d]azepin-2[1H]-yl)-2-methylprop-2-en-1-one) (piBOHPAMP), and poly(N-(3-((1-benzylpiperidin-4-yl)oxy)propyl)acrylamide) (pBPOPAm), and these are found to adsorb virions. However, due to limitations in the diversity of structures in the training set, the computational models are unable to predict the adsorption of virions for all polymer structures. Summarily, these findings indicate the utility of the methodology to identify coating polymers that effectively immobilize SARS-CoV-2, with potential practical applications (e.g., water and air filtration).

INTRODUCTION

Severe acute respiratory syndrome coronavirus 2 (SARS-CoV-2), the causative agent of coronavirus disease 2019 (COVID-19), has caused a global public health emergency. Like other human respiratory viruses, SARS-CoV-2 is transmitted through direct inhalation of virus-laden droplets or, more rarely, aerosols or by hand contact with contaminated surfaces and subsequent transfer to mucus membranes.¹ In addition to being spread through the air,² the virus may also migrate via other routes. For example, SARS-CoV-2 virions have been found in wastewater, and their numbers correlate strongly with epidemic growth rates.³ The best long-term population-wide approach to combating viral infections is to prevent infection through a good public health environment. Therefore, it is important to develop effective strategies to improve water and air quality and, thus, reduce virus exposure routes for better infection control.

¹Division of Advanced Materials and Healthcare Technologies, School of Pharmacy, University of Nottingham, Nottingham NG7 2RD, UK

²Department of Chemistry, School of Science, Xi'an Jiaotong - Liverpool University, Suzhou 215123, P.R. China

³School of Life Sciences, University of Nottingham, Queen's Medical Centre, Nottingham NG7 2UH, UK

⁴Wolfson Centre for Research on Global Virus Infections, University of Nottingham, Queen's Medical Centre, Nottingham NG7 2UH, UK

⁵Division of Molecular Therapeutics and Formulation, School of Pharmacy, University of Nottingham, Nottingham NG7 2RD, UK

⁶Nottingham Biomedical Research Centre, University of Nottingham, Queen's Medical Centre, Nottingham NG7 2UH, UK

⁷Lead contact

*Correspondence: xuan.xue@xjtlu.edu.cn (X.X.), morgan.alexander@nottingham.ac.uk (M.R.A.)
<https://doi.org/10.1016/j.xcrp.2024.102204>



Applying effective water and air purification processes to remove biological contaminants, including viruses, would benefit public health and reduce viral transmission. Existing technologies applied for this purpose include membrane bioreactor systems,⁴ photocatalytic disinfection,⁵ UV irradiation,⁶ and membrane-based filtration.^{7,8} Among them, membrane-based filtration via virus particle adsorption has attracted particular attention due to its high removal efficiency and low cost. A range of adsorbent materials have been exploited in filtration membranes against virus contamination in water, including carbon-based, silicon-based, oxide-based, metal-based, and carbohydrate materials, which may be further extended and developed for air purification.⁹ While limitations to their wide use have been proposed, simple polymers have shown advances if exploited to this aim, such as environmental friendliness, non- or low-contact cytotoxicity, long durability, low cost, and, in particular, the broad variety of surface chemistries offered by polymers,¹⁰ In fact, there is an opportunity to discover polymers that are specifically designed to immobilize virions by adsorption, and ideally also accelerate virus inactivation, for potential applications in air and water filtration, personal protective equipment (PPE), the built environment, and consumer products.

To date, the theoretical basis for describing viral particle interactions at synthetic surfaces is not sufficiently well developed to allow performance prediction to guide new polymer development.¹¹ One means of identifying materials that does not require such a theoretical framework and could help to build one is to use high-throughput polymer microarray screening. High-throughput materials discovery using polymer microarrays has mainly been explored in identifying bioinstructive polymers to control bacterial biofilm formation,¹² stem cell pluripotency,¹³ and phenotype control.¹⁴ Moreover, high-throughput polymer microarray screening combined with predictive quantitative structure-activity relationships (QSARs) has been exemplified for the discovery of novel materials,^{15,16} which may be adopted to the development of new virion adsorbent polymer materials. In fact, direct discovery of virucidal materials using polymer microarray screening has been excluded due to difficulties in the recovery of live virus from polymer spots within a microarray and the subsequent quantification of the infectious virions using the traditional quantitative methods (e.g., 50% tissue culture infective dose (TCID₅₀) endpoint titration and viral plaque assays).

While host infection starts from virus attachment to cells by recognition and binding events with surface receptors, viral attachment to manmade surfaces is expected to be a function of the physicochemical properties of the material. The binding of viruses on synthetic surfaces has typically been described using non-specific electrostatic^{17–20} and hydrophobic^{18–21} interactions. In addition, some studies have demonstrated that strong irreversible adsorption on hydrophobic and polycationic surfaces damaged and inactivated viruses.^{18–20} These findings suggest that surface binding may be the first step of virus inactivation at the material surface. Recent work in screening polymer libraries using microarrays for rubella and Lassa fever virus-like particles demonstrated the potential of polymer microarray screening in differentiating materials with binding affinities to the virus.²² Herein, high-throughput screening of strong virion-binding polymers is expected to narrow the number of candidate polymers for virucidal evaluation, which is limited to low-throughput screening, and, at the same time, provide the opportunity to identify the virion adsorbent polymers with potential practical applications.

The aims of this research are to discover polymers that strongly bind viral particles and evaluate their virucidal performance as selection criteria to identify new coating

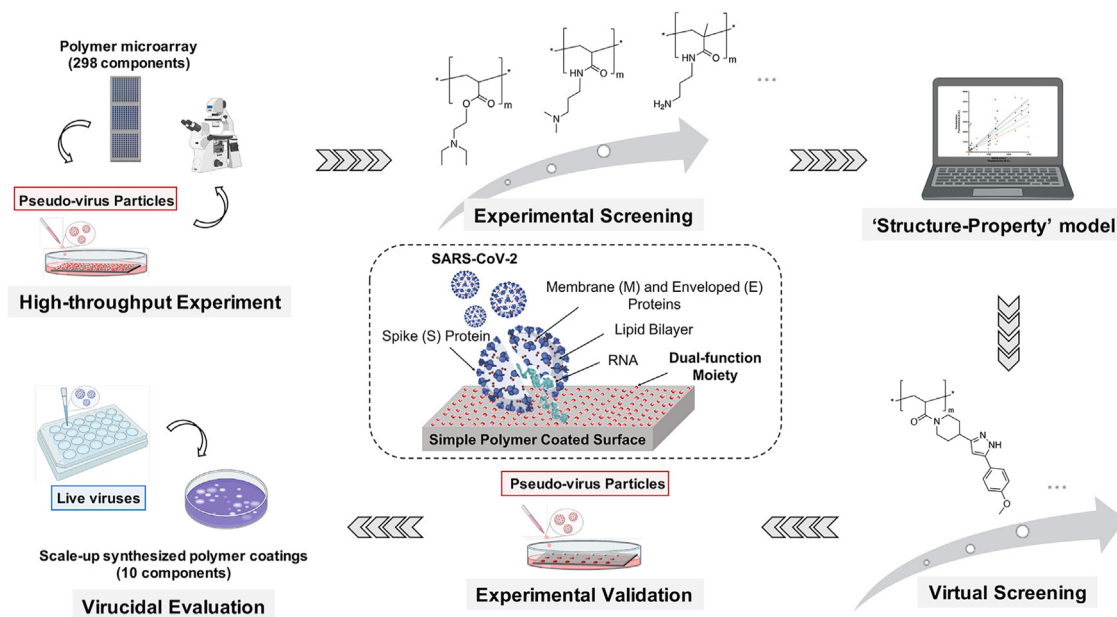


Figure 1. Schematic representation of the process for the discovery of coating polymers that effectively immobilize SARS-CoV-2

298 commercially available materials are assessed for their ability to bind virions via high-throughput screening using pseudo-virus particles, processed data are used to identify polymer candidates within the existing library, analyzed data together with material chemical structures are used to generate computational models that predict new untested materials, candidates from the virtual screening are then validated through pseudo-virus adsorption experiments identical to the high-throughput experiments, and polymer candidates determined via both experimental and virtual screening are then scale-up synthesized and coated on glass coverslips for further virucidal evaluation using live SARS-CoV-2 system.

polymers. The study starts from a pseudo-virus particle adsorption assay in water using a polymer microarray containing 298 polymer chemistries, the results of which are then used to screen the virion adsorbent polymers within this existing library and discover new strong virion-binding structures generated by the computational model. Polymer candidates determined via both experimental and virtual screening are then scale-up synthesized and applied to form coating surfaces for virucidal evaluation using an *in vitro* infectious live SARS-CoV-2 system (Figure 1).

RESULTS AND DISCUSSION

Discovering strong virion-binding polymers

High-throughput adsorption assays were performed using polymer microarrays and Alexa Fluor 647-labeled retroviral SARS-CoV-2 pseudo-virus particles, which can be handled without heightened biological containment measures due to their non-infective nature. The polymer microarrays used in this study were fabricated by contact printing and subsequent *in situ* photopolymerization of an array of 298 monomer compositions (296 homopolymers and 2 copolymers) onto an epoxy-functionalized, poly(2-hydroxyethyl methacrylate) (pHEMA)-coated glass slide in triplicate, as described previously.^{12–14} The pHEMA coating reduces binding to the background array surface. The slide preparation method and the identity of the 298 polymers are detailed in the [supplemental information \(supplemental experimental procedures; Figure S1; Data S1\)](#). This polymer microarray was designed to cover a wide range of chemistries provided by commercially available monomers to maximize the chemical diversity of the array system for unbiased screening and help build a structure-property model for future structure prediction. The polymer microarray was incubated in assay solution (pseudo-virus suspension) in the dark to reach an equilibrium adsorption.²² Fluorescence images of the microarray were acquired

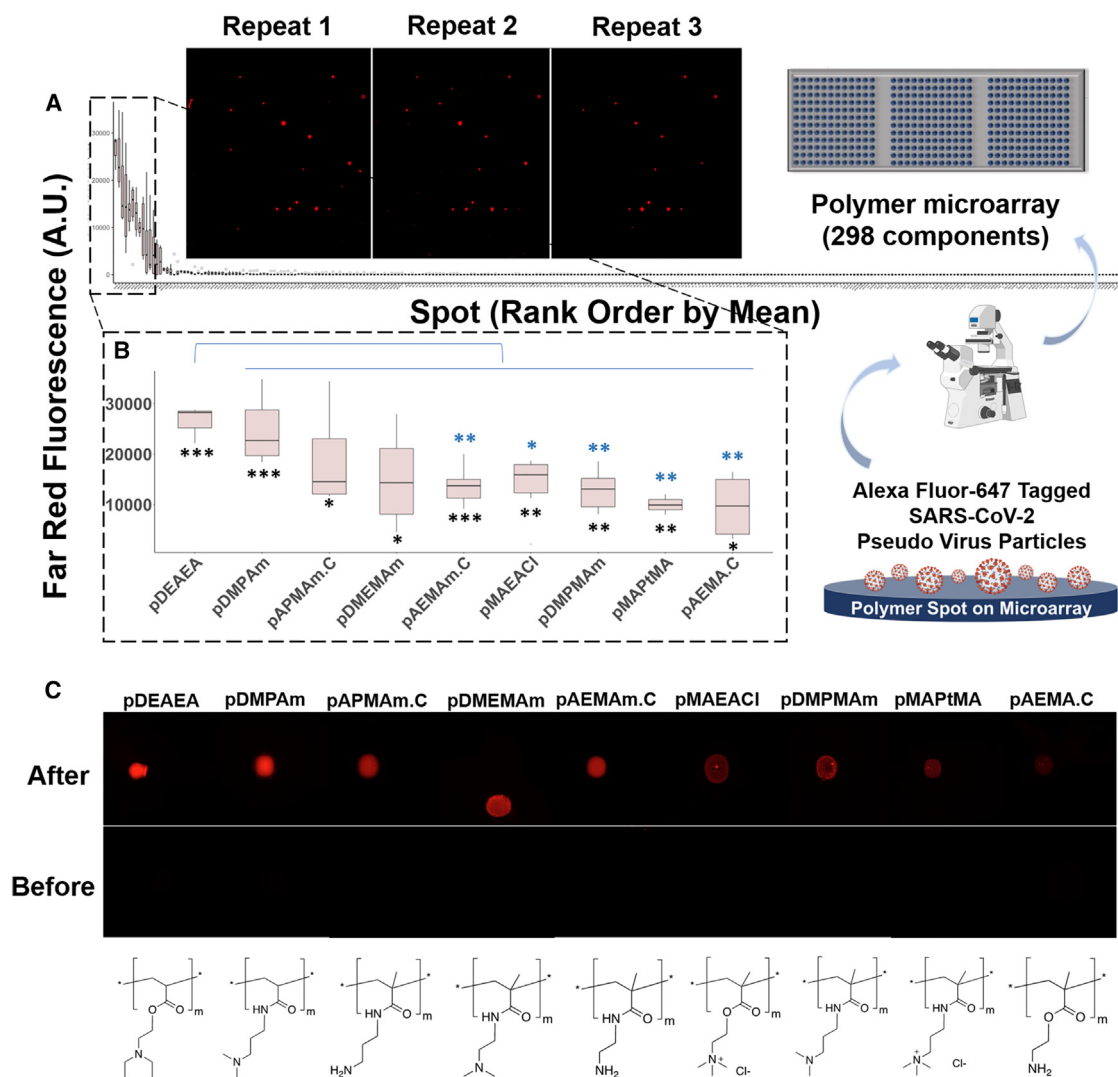


Figure 2. Experimental results of polymer microarray adsorption assay using Alexa Fluor 647-tagged SARS-CoV-2 pseudo-virus particles

(A) Polymer microarray was designed and printed with triplicate arrays on one glass coverslip and 298 polymer chemistries in each array. The adsorption assay was carried out with three experimental repeats and two biological repeats ($n = 6$). The mean fluorescence intensity per pixel for each spot was rank ordered to identify polymers with strong adsorption against SARS-CoV-2 pseudo-virus particles.

(B) The polymers with the highest fluorescent intensity. Statistical analysis by using Student's t test has been carried out between the substrate (pHEMA) and the top 9 polymers (the number of stars in black below the data box indicates the significance of the difference) and between the best "hit" pDEAEA and the other 8 polymers (the number of stars in blue above the data box indicates the significance of the difference) ($*p < 0.05$, $**p < 0.01$, $***p < 0.001$, and $****p < 0.0001$).

(C) Representative microscope images of the top 9 polymers, significantly different from the substrate adsorption, to show the fluorescence difference before and after the assay due to SARS-CoV-2 pseudo-virus particle adsorption.

both before and after incubation (further details of pseudo-virus particle preparation and assay conditions can be found in the [experimental procedures](#) section and the [supplemental information](#)).

After incubation, there was visible fluorescence intensity observed on some of the printed spots, indicating adsorption, as shown in [Figure 2A](#); a representative scan of one full glass slide included triplicate arrays for experimental repeats, where a reproducible pattern due to adsorption was observed. Two polymer microarray glass slides were used in two separate experiments for biological repeats. A

Table 1. List of polymers showing the highest binding to SARS-CoV-2 pseudo-virus particles

No.	Polymer name	Abbreviation
1	poly(2-diethylamino) ethyl acrylate)	pDEAEA
2	poly(N-[3-(dimethylamino) propyl] acrylamide)	pDMPAm
3	poly(N-(3-aminopropyl) methacrylamide hydrochloride)	pAPMAm.C
4	poly(N-[2-N,N-dimethylamino]ethyl] methacrylamide)	pDMEMAm
5	poly(N-(2-aminoethyl) methacrylamide hydrochloride)	pAEMAm.C
6	poly([2-(methacryloyloxy) ethyl] trimethylammonium chloride)	pMAEACl
7	poly(N-[3-(dimethylamino) propyl] methacrylamide)	pDMPMAm
8	poly(methacrylamido propyl trimethyl ammonium chloride)	pMAPtMA
9	poly(2-aminoethyl methacrylate hydrochloride)	pAEMA.C

fluorescence image was acquired at each spot position listed on the array to acquire high-sensitivity and lateral-resolution data, where the mean fluorescence intensity per pixel of each spot of 3 replicates of each 298 chemistries are rank ordered as shown in the profile in Figure 2A. The highest binding polymers identified are listed in Table 1, and shown in Figure 2B with statistical analysis, compared to the pHEMA substrate (black *) and the strongest binder in this experimental screen, poly(2-diethylamino) ethyl acrylate) (pDEAEA) (blue *). Representative fluorescence images and chemical structures of the top polymers are shown in Figure 2C.

In general, amine functionalities were found to be common structures in all these polymers, leading to the hypothesis that the strong binding is dominated by electrostatic interactions between the charged amines of the polymers and the moieties on the SARS-CoV-2 pseudo-virus particle outer surface. Specifically, SARS-CoV-2 is an enveloped coronavirus, in which the viral nucleocapsids are encapsulated in a phospholipid bilayer with embedded structural proteins, such as membrane protein, envelope protein, and spike glycoprotein (S protein).²³ The phospholipid bilayer imparts a negative surface charge and hydrophobic properties. The S protein, which consists of more than 1,000 amino acids, is located on the surface of SARS-CoV-2 and assembled into crown-like nano-objects for the virus to bind and fuse with the host cell membrane via the ACE2 receptor.²⁴ The isoelectric point (PI) of virions is an important characteristic value in identifying electrostatic interactions at a given pH and, therefore, contributes to their adsorption strength with surfaces. The S protein is reported to exhibit a PI of 5.9,¹⁸ and the PI of SARS-CoV-2 was measured to be 5.2–5.3.²⁵ The surface charge on pseudo-virus particles and polymer surfaces depends on the environmental pH: the pH values of the assay solutions, obtained by resuspending the stock solution in Milli-Q water, were measured to be 7.4 (Figure S2A). In the assay solution, the adsorbates are expected to be negatively charged, which was also demonstrated in the direct measurements of the zeta potential (Figure S2B). In addition, while the pK_a values of most simple alkyl amines are above 9, when combined as multiple side chains within a polymer, the local environment is different due to the presence of multiple numbering ionic species.^{26,27} Accordingly, the pK_a values of some of the amine-pendent polymers were determined by titration experiments in Milli-Q water at room temperature and found to be in the range of 7–8 as reported.^{28–30} Thus, the microarray spots of amine-pendent polymers were expected to be positively charged due to protonation under the assay condition. It is therefore likely that in the presence of the conditions we employed, non-specific electrostatic binding contributed most significantly to the adsorption.

However, in addition to electrostatic interactions, other intermolecular forces at SARS-CoV-2 surface moieties may, to some extent, contribute to the overall adsorption of virion on polymer surfaces. As observed in Figure 2C, the best adsorbents show a high degree of structural similarity but slightly different adsorption properties, where the role of hydrophobic associations and hydrogen bond donor and acceptor interactions may contribute, especially when the overall PI values of these polymers are quite close. For example, hydrophobic moieties within the S protein and the hydrophobic membranes of the viral phospholipid bilayer might interact with aryl or alkyl chains attached to the surface polymer amines.³¹ It is also known that longer alkyl chains attached to the tertiary amine nitrogen can lower the pK_a of the resulting polymer.³² Additionally, the permanently charged ammonium derivatives pMAEACI and pMAPtMA showed slightly less virion binding than pDEAEA, possibly due to local repulsive charge-charge interactions at S protein lysine and arginine and the lack of hydrogen-bonding interactions between the quaternary amine and other amino acid side chains (e.g., tyrosine and asparagine) in the S protein, while other types of amines retain the potential to establish this additional non-covalent interaction.³² These results suggest that the overall adsorption is the coordinated result of multiple intermolecular interactions between virions and inanimate surfaces.

Moreover, the actual binding is also closely related to the type and distribution of the functional moieties on the virion surface and those on the polymer surfaces. For instance, N-[2-N,N-dimethylamino]ethyl] methacrylamide (DMEMAm) and N-[3-(dimethylamino) propyl] methacrylamide (DMPMAm) have only a single carbon spacer difference, but a clear difference in their polymers' adsorption performances is observed, as shown in Figure 2C, which may be attributed to the number of effective interactions able to be established between the surface moieties of the SARS-CoV-2 virion and those on polymeric substrates. These hypotheses were also supported by the experimental high-throughput screening results with other types of pseudo-virus particles (Figure S2C), where the top performers were more or less the same as those with SARS-CoV-2 due to the dominating electrostatic interaction, while the detailed orders were different from each other, possibly due to the differences in composition, density, and distribution of the surface moieties of the virions and the fine-tuning of intermolecular interactions (e.g., hydrophobic, hydrogen binding, and possibly van der Waals forces³³) with the polymer surface chemistries.

To understand better the intermolecular interactions that contribute to virion adsorption on polymeric substrates, computational models were developed where the virtual screening results further supported the proposed mechanisms (see the next section for details).

Developing a model of virion binding to polymers using molecular descriptors: Virtual screening

The attachment data generated from the microarrays were used to develop polymer structure-property models using machine learning to enable the prediction of new polymers able to promote virion adsorption from a virtual monomer library comprising commercially available compounds. Each polymer was approximated using its monomeric unit represented by an SMILES string,³⁴ and descriptors were generated from these using the Python cheminformatics library RDKit (v.2021.09.4)³⁵ (RDKit³⁶: Open-Source Cheminformatics Software, <http://www.rdkit.org/>). Classification was used as a computational approach to model the adsorption response of the homopolymers in the dataset. The class cutoff was set to 2 fluorescent a.u. (Figure S3), which provided a good compromise between

needing to set the cutoff as close to zero as possible and guaranteeing a good representation of the class exhibiting no attachment: the first condition was crucial to allow models to mimic the observed adsorption behavior, thus assigning all those non-adsorbing polymers the class 0; the second condition was needed to avoid or mitigate the class imbalance that could lead to model bias. The dataset was split into training and test sets with a fixed random seed (80% training set, 20% test set). However, the under-sampling process led to a final 50/50 class balance in the training set, while the test set remained unaffected (Table S1). Before building any machine learning model, descriptors were filtered out to discard those highly correlated and with low diversity^{16,37}: filtering by multicollinearity was necessary to avoid redundant information that could carry some noise, while filtering by diversity was necessary to enable all descriptors to carry a minimum accepted amount of information. The obtained descriptor list was then passed to two different learning approach pipelines to establish two separate models (Figures 3A; supplemental experimental procedures).

Two models were found to outperform the others tried. The first, model A, was a simple logistic regression (LR) model with two combined molecular descriptors. The model was iteratively trained on a large number of small feature subsets combinatorially generated from the descriptor list and was validated via a 5-fold stratified cross-validation. Specifically, model A was generated by applying multicollinearity and diversity thresholds to $|r| = 0.8$ ($r^2 = 0.64$) after a second-degree expansion of the 208 RDKit descriptors, and an LR model with an L2 penalty (also called Ridge regularization) and a regularization strength of 1 was used to explore the performance of the multiple feature subsets generated by the combinatorial approach. The feature subset returning the best training, cross-validation, and test scores was chosen as the final descriptor for model A. Such a model was able to predict the virion attachment response with a training Matthew's correlation coefficient (MCC) = 0.40, a cross-validation MCC = 0.42 ± 0.18 , and a test MCC = 0.40. Sensitivity and specificity were 0.72 and 0.75, respectively. This model was simple; however, the performance metrics are satisfactory, and the MCC does not vary between training, cross-validation, and test phases, which demonstrated the overall robustness and generalization ability of the model. Model A, when applied to the test set, returned 31 true positives, 9 true negatives, 3 false positives, and 12 false negatives, with a Fisher's exact test $p < 0.01$. The combined descriptor $MinEStateIndex * VSA_{EState8}$ positively correlated with the adsorption, while the descriptor $BCUT2D_{CHGLO}$ was anti-adsorption (Figure 3B).

The second model, model B, was an LR model with eight combined molecular descriptors obtained through a sequential forward selection (SFS) algorithm, which includes a stratified, 10-fold cross-validation carried out at each iteration. Specifically, model B was generated by applying multicollinearity and diversity thresholds set to $|r| = 0.7$ ($r^2 = 0.49$) after a second-degree expansion of the 208 RDKit descriptors and an LR model with an L1 penalty (also called Lasso regularization) and a regularization strength of 1. Model B was able to predict the virion adsorption response with a training MCC = 0.46, a cross-validation MCC = 0.50 ± 0.25 , and a test MCC = 0.45. Sensitivity and specificity were 0.77 and 0.75, respectively. This model had 8 descriptors but is still relatively simple, and its predictive ability was a strict upgrade from model A, as can be seen from the confusion matrices (Figure S4). Model B, when applied to the test set, returned 33 true positives, 9 true negatives, 3 false positives, and 10 false negatives, with a Fisher's exact test $p < 0.01$. Among all 8 descriptors used, the 3 descriptors with a pro-adsorption coefficient were $FpDensityMorgan1 * Chi0v$, $MaxEStateIndex$, and $BalabanJ * PEOE_{VSA6}$, while the 4 descriptors showing an anti-adsorption contribution

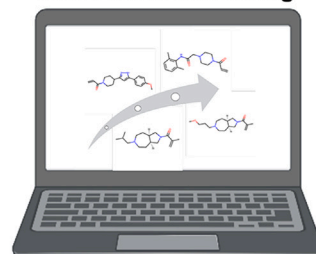
A

Model name	Diversity, r thresholds	Regularizing term	Descriptors	Training MCC	Mean CV MCC (p-value)	Test MCC	Sens	Spec	G-mean
Model A (Combinatorial)	0.8 after expansion	L2, 1	2	0.40	0.42±0.18 (<10 ⁻²)	0.40	0.72	0.75	0.74
Model B (SFS)	0.7 after expansion	L1, 1	8	0.46	0.50±0.25 (<10 ⁻⁴)	0.45	0.77	0.75	0.76

B

Model name	Feature	Weight	Normalized weight
Model A	<i>MinEStateIndex * VSA_EState8</i>	0.73	62.84%
	<i>BCUT2D_CHGLO</i>	-0.43	-37.16%
Model B	<i>BCUT2D_MW HI * EState_VSA2</i>	-0.46	-22.46%
	<i>FpDensityMorgan1 * Chi0v</i>	0.38	18.40%
	<i>Ipc * PEOE_VSA9</i>	-0.36	-17.66%
	<i>MinAbsEStateIndex * SlogP_VSA3</i>	-0.33	-16.38%
	<i>MaxEStateIndex</i>	0.25	12.11%
	<i>MaxPartialCharge * BCUT2D_MWLOW</i>	-0.18	-8.73%
	<i>Balabanj * PEOE_VSA6</i>	0.09	4.27%
	<i>FpDensityMorgan1 * fr_ester</i>	0.00	0.00%

Computational Modelling and Virtual Screening



C

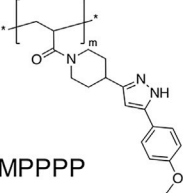
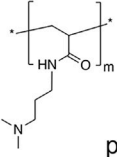
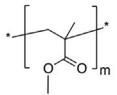
Monomer structures	Probability (P) of Being Pro-adsorption	Binding Category
 <p>pMPPPP</p>	0.8355	High
 <p>pDMPAm</p>	0.6549	Medium high
 <p>pMMA</p>	0.4000	Low

Figure 3. Computational models and representative virtual screening results

(A) Summary of classification model performances. The columns indicate, respectively, the name of the model; the threshold used for multicollinearity and diversity filters; the regularizing term of the model; the number of descriptors and their nature; the training, cross-validation (with a *p* value after doing a one-sample, single-tailed *t* test for the score > 0), and test MCCs; and the sensitivity, specificity, and geometric mean of sensitivity and specificity.

(B) The RDKit descriptors used by model A and model B with their true and normalized weights.

(C) Representative virtual screening results of March 2022 Molport in-stock catalog: the monomers were rank ordered by their probability (*p* values) of being pro-adsorption against SARS-CoV-2 pseudo-virus particles.

were $BCUT2D_{MWHI} * EState_{VSA2}$, $lpc_{PEOE_{VSA9}}$, $MinAbsEStateIndex * SlogP_{VSA3}$, and $MaxPartialCharge * BCUT2D_{MWLOW}$. The descriptor $FpDensityMorgan1 * fr_{ester}$ had no weight, due to the L1-penalized LR algorithm inside the SFS method setting this descriptor coefficient to zero at a later time, after the wrapper itself had included it in the first place (Figure 3B).

Both models were able to assign the adsorption class of polymers with good predictive power and were statistically significant. Both models showed that a link between the material chemistry and the viral binding performance existed. However, molecular descriptors are often arcane and provide little or no insight into the mechanism beyond the identification of a link between materials chemistry and binding. Even though the interpretability process can be hampered by models whose features do not have an immediate meaning, virtual screening can still be carried out to look for new promising structures. The virtual screening was then applied to the March 2022 Molport in-stock catalog, and RDKit descriptors used by the obtained models were computed on all compounds having an acrylic moiety (thus both [meth]acrylates and [meth]acrylamides) within the applicability domain of the models, which was computed using the leverage method as described elsewhere.^{38,39}

Representative polymers from the high, medium, and low binding categories by virtual screening and their probability (p value) of being pro-adsorption are shown in Figure 3C, where the p values reported are the average of the probability values generated by the two models (A/B). Specifically, poly(1-{4-[5-(4-methoxyphenyl)-1H-pyrazol-3-yl]piperidin-1-yl}prop-2-en-1-one) (pMPPPP), which was not included in the existing polymer library, was predicted to exhibit strong virion binding due to the high probability ($p = 0.8355$) of being pro-adsorption, determined by the virtual screening; poly(N-[3-(dimethylamino)propyl]-acrylamide) (pDMPAm) and poly(methyl methacrylate) (pMMA) were a strong and a non-virion binder, respectively, in the existing polymer library, as determined by the experimental screening (Figures 2B and 2C), which was in good agreement with the $p = 0.6548$ (medium high) and 0.4000 (low), respectively, determined by the virtual screening. The full results can be found in Data S2.

In general, the chemical structures of the predicted pro-adsorption hits had recurrent moieties or functional groups, for example, nitrogen-containing structures such as amide polymer main-chain backbones, nitrogen-containing heterocycles, and primary and tertiary amines, which are positively charged in nature at a physiological pH. Such moieties are also displayed with linear and/or cyclic alkanes and/or aromatic rings. These virtual screening results suggested that the combined features could provide electrostatic and hydrophobic interactions with negatively charged hydrophobic SARS-CoV-2 virions.^{17,20} Moreover, such interactions are particularly enhanced when tertiary amines and aromatic rings exist in the same monomer, as observed in the best pro-adsorption structures, possibly due to the “synergy effect” arising from the π - π stack³² region, which further enhances the hydrophobic interaction once the protonated tertiary amines initiate the process via electrostatic interactions.

Testing the validity of the models

Subsequently, pMPPPP, predicted to give strong virion binding by the virtual screening, was experimentally evaluated by comparing it with pDMPAm, as a positive comparator, and pMMA, as a negative comparator, using the same adsorption assay as previously described, with the adaption that the polymer spots are $\sim 500 \mu\text{m}$ in diameter. As shown in Figure 4A, pMPPPP surfaces adsorbed a higher amount of

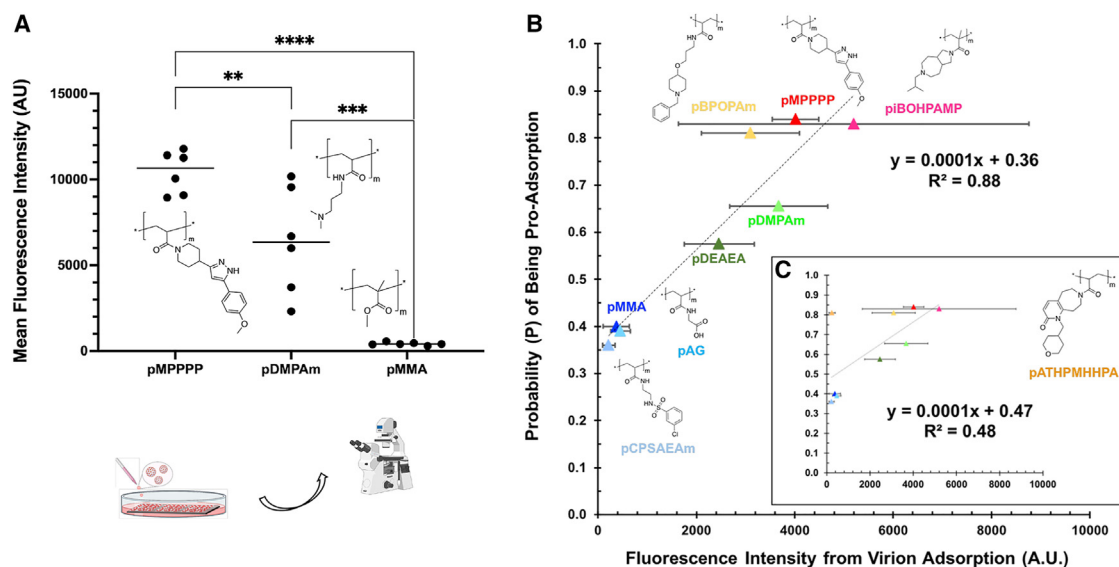


Figure 4. Experimental results on the validity of the models

(A) Experimental adsorption assay with Alexa Fluor 647-tagged SARS-CoV-2 pseudo-virus particles. A polymer microarray was printed on one glass coverslip with six spots ($n = 6$) for each polymer chemistry, including the best structure MPPPP produced by regression model virtual screening; the pDMPAm polymer gave the highest adsorption based on the high-throughput results to compare with pMPPPP polymer; the pMMA polymer did not adsorb pseudo-virus particles as negative control. The mean fluorescence intensity per pixel for each spot, due to the adsorption of SARS-CoV-2 pseudo-virus particles, was measured. (background autofluorescence has been deducted in all cases). A significant difference was observed between pMPPPP and pMMA ($**p < 0.01$) and between pDMPAm and pMMA ($*p < 0.05$) by one-way ANOVA Dunnett's test.

(B and C) Testing of the computational models with additional selections from the virtual screening results, including three pro-adsorption polymers, poly(1-(6-isobutylloctahydropyrrolo[3,4-d]azepin-2[1H]-yl)-2-methylprop-2-en-1-one) (piBOHPAMP), poly(*N*-(3-((1-benzylpiperidin-4-yl)oxy)propyl)acrylamide) (pBPOPAm), and poly(7-acryloyl-1-((tetrahydro-2H-pyran-4-yl)methyl)-1,5,6,7,8,9-hexahydro-2H-pyrido[2,3-d]azepin-2-one) (pATHPMHHPA), and two anti-adsorption polymers, poly(*N*-(2-((3-chlorophenyl)sulfonamido)ethyl)acrylamide) (pCPSAEAm) and poly(acryloylglycine) (pAG), using experimental adsorption assay with Alexa Fluor 647-tagged SARS-CoV-2 pseudo-virus particles ($n = 6$). The experimentally measured fluorescent intensity due to virion binding was plotted against the model-predicted probability (P) of being pro-adsorption, where a simple linear regression equation was generated with (B) an R^2 value of 0.88 and (C) an R^2 value of 0.48 when pATHPMHHPA was included in analysis.

Alexa Fluor 647-tagged SARS-CoV-2 pseudo-virus particles compared to the positive control pDMPAm screened from the existing library and a significantly higher amount than that of the negative control, pMMA ($**p < 0.01$), which confirmed the successful discovery of a new, strong virion-binding material and demonstrated a valid structural prediction by the established models.

To further test the prediction capability of the models, additional selections from the virtual screening result were polymerized and tested. These included three pro-adsorption polymers: poly(1-(6-isobutylloctahydropyrrolo[3,4-d]azepin-2[1H]-yl)-2-methylprop-2-en-1-one) (piBOHPAMP), poly(*N*-(3-((1-benzylpiperidin-4-yl)oxy)propyl)acrylamide) (pBPOPAm), and poly(7-acryloyl-1-((tetrahydro-2H-pyran-4-yl)methyl)-1,5,6,7,8,9-hexahydro-2H-pyrido[2,3-d]azepin-2-one) (pATHPMHHPA). Two anti-adsorption polymers were also included: poly(*N*-(2-((3-chlorophenyl)sulfonamido)ethyl)acrylamide) (pCPSAEAm) and poly(acryloylglycine) (pAG). The results from these are compared to the best pro-adsorption polymers, pDEAEA and pDMPAm, and the anti-adsorption polymer, pMMA, from the existing library in Figure 4B, where the experimentally measured fluorescent intensity was plotted against the model-predicted probability (P) of being pro-adsorption.

Among the polymers used to test the predictive ability of the model, pro-adsorption polymer pATHPMHHPA, identified in the virtual screen, showed low virion adsorption as indicated by the fluorescent intensity of the assay results. Consequently,

the linear regression equation (best fit) resulted in an R^2 value of 0.48, which suggests a weak correlation between the actual and predicted screening results (Figure 4C). This may be because the nitrogen in the structure of pATHPMHHPA exists in the form of an amide rather than an amine and, thus, is not protonated under the assay conditions (the amide nitrogen is not basic), whereas the model assumed the presence of “nitrogen” equals “high adsorption” in the absence of a fuller training set, resulting in a poor prediction of this polymer. When the pATHPMHHPA data were removed from the simple linear regression equation, it resulted in an R^2 value of 0.88 (Figure 4B), confirming its impact. This indicates a limitation in the model in that pATHPMHHPA contains functional chemistries, e.g., a cyclic amide in the side chain, which is a feature beyond that of the input dataset, which predominantly included neutral hydrophobic and amine-functional structures.

These findings indicate that the models have the predictive power to discover strong virion-binding polymers but are limited by the depth of the training set data. To improve the models’ predictive power, more functionally diverse surfaces (with amines of a range of pKa) and multiple types of pseudo-virus particles should be included in larger datasets for machine learning and to build real “AI” models in future studies.

Live-virus viability on materials chosen from high pseudo-virus binders

Postulating that viral attachment to manmade surfaces is the first step toward virus-surface interaction and thus a strong binding polymer may result in an increased virus inactivation, polymers found to be strong pseudo-virus adsorbers were scaled up for live SARS-CoV-2 testing. Candidates that readily formed gels were excluded at this stage due to their likely low durability on high-touch surfaces. pDEAEA, pDMPAm, pDMEMAm, pMAEACl, pDMPMAm, and pMAPtMA were taken forward as candidates, and pMMA was chosen as non-virion-binding comparator to be synthesized using free radical polymerization in solution to allow full polymer purification and characterization. In comparison to UV *in situ* curing, this also allows macroscopic films to be readily cast without the retention of undesirable residual monomers (Table S2). The polymers were then dissolved and coated on glass coverslips for virucidal evaluation. Virus stock containing 7.2×10^3 (equal to 3.9 log units) TCID₅₀ of SARS-CoV-2 was inoculated on each 1×1 cm² polymer. After a 10 min incubation under ambient conditions, the viral load recovered from each material was determined by the TCID₅₀ assay and compared to a polystyrene (PS) surface (non-treated tissue culture well plate) as the control to give a percentage of viral degradation attributed to the presence of the material sample (Figure 5). By doing this, any loss of virus due to experimental procedures and natural virus decay outside a host was taken into account.

After 10 min direct contact with polymer-coated surfaces, the proportions of viable SARS-CoV-2 recovered from pDEAEA, pDMPAm, pDMEMAm, pMAEACl, pDMPMAm, and pMAPtMA were 7.7%, 263.3%, 44.3%, 29.3%, 75.8%, and 34.8%, respectively, while those of the uncoated glass (substrate for polymer coating) and pMMA (non-virion binding, negative control) were 212.0% and 345.0%, respectively. The result of pMPPPP (model virtual screening “hit”) was 204.8% (Figure 5). In brief, the proportions of viable SARS-CoV-2 recovered from all test materials were calculated and then analyzed using one-way ANOVA Dunnett’s multiple comparisons test to compare with the PS control and evaluate the statistical difference. Significant loss of SARS-CoV-2 was observed following contact with pDEAEA-coated glass as compared to PS control ($*p < 0.05$), uncoated glass ($**p < 0.01$), pDMPAm ($***p < 0.001$), and pMMA ($**p < 0.01$) respectively. Also, pDEAEA

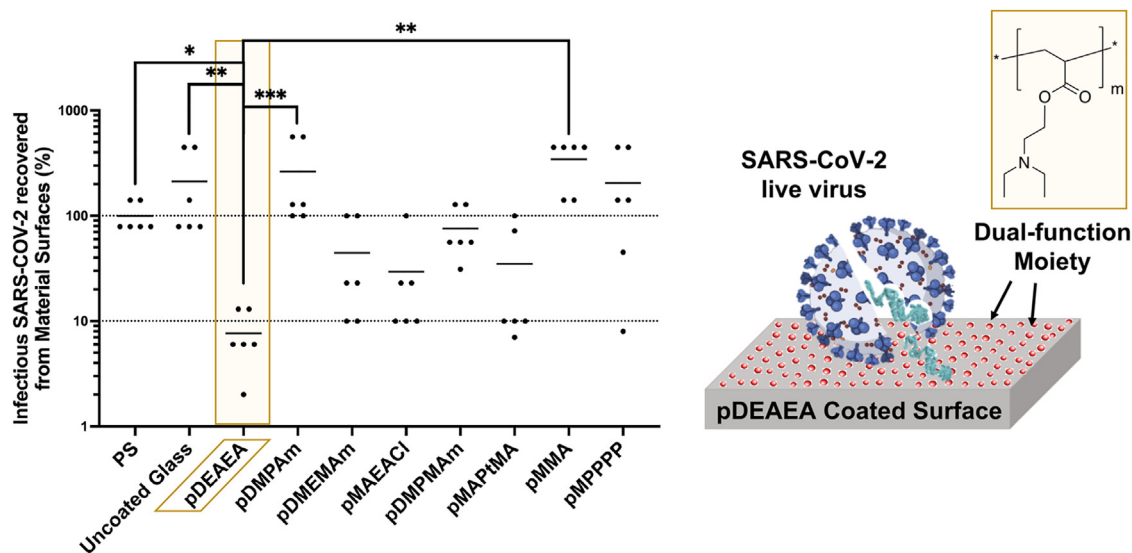


Figure 5. Experimental results of virucidal performance of “hit” polymers selected by high-throughput screening and the computational model using live SARS-CoV-2

Experimental inoculation of SARS-CoV-2 was kept on polymer surface for 10 min incubation ($n = 6$). The viral load recovered from the surfaces was quantified by $TCID_{50}$ endpoint titration and viral plaque assay; one dot represents the result obtained from one experimental repeat. Significant differences were found between the pDEAEA coating surface and PS control ($*p < 0.05$), uncoated glass ($**p < 0.01$), pDMPAm ($***p < 0.001$), and pMMA ($**p < 0.01$), respectively, in the 10 min incubation, by one-way ANOVA Dunnett’s test.

coating demonstrated more than 10-fold virus reduction within 10 min upon contact, which is comparable to that of a commercially available product (Virustatic Shield⁴⁰; 10-fold virus reduction within 10 min) evaluated in our previous study.⁴¹ In advance of field trials, this provides some indication that the pDEAEA polymer can be viewed to be virucidal under the test condition, and its comparable performance to a commercial product that utilizes protein coating suggests that a purely synthetic solution could be beneficial. No significant difference was observed between any other two materials.

Considering the mechanism hypothesized from the experiments along with the descriptors derived from the modeling, the positive charge and/or hydrophobic nature at a physiological pH of the material surfaces are expected to interact strongly with negatively charged hydrophobic SARS-CoV-2 virions^{18,25} via electrostatic and hydrophobic interactions, which agrees with previous studies.^{17,20,42} These interactions contribute significantly to the binding between the virions and material surfaces and virus inactivation due to the irreversible binding-induced virion structure damage.²⁰ However, except for pDEAEA, none of the pro-adsorption polymers screened from the existing library, nor those predicted from the computational model, meet the requirement to be classed as virucidal. The live-virus titer data indicate that there is no correlation between pseudo-virus particle binding and SARS-CoV-2 viral inactivation for the top 5 binders shown in Figures 2A and 5, with the exception of pDEAEA. This indicates that inactivation and binding are not related in the simple manner initially proposed. Further studies focusing on the theoretical basis for describing virion interactions at surfaces are required to investigate this.

Conclusions

Polymers that promote virion binding have been discovered by quantifying the adsorption of pseudo-virus particles in high-throughput adsorption assays using

polymer libraries presented on microarrays, where non-specific electrostatic binding dominates the interactions between the particles and polymer surfaces, while other intermolecular interactions (hydrophobic, hydrogen bonding, and van der Waals forces) contribute to the fine-tuning of the adsorption.

Two classification models were established to carry out a consensus virtual screening. A list of the best structures was produced from them to indicate a recurrent molecular scheme, which was experimentally validated with the best virtual structures (pMPPPP, piBOHPAMP, and pBPOPAm) and the worst ones (pCPSAEAm and pAG) using an adsorption assay. However, when testing amide structures (e.g., pATHPMHHPA) instead of amines, the predictive power of the models was exceeded. These findings demonstrate that the models have the predictive power to discover strong virion-binding polymers but only at a simple level of electrostatic binding interactions. There are opportunities to use larger datasets and machine learning methods to improve the models and evaluate more fully the mechanisms behind them in future studies.

In addition, the pDEAEA polymer was found to be effective as an anti-viral surface through virucidal evaluation of the best virion-binding polymers, where a 10-fold SARS-CoV-2 reduction was observed within 10 min upon contact. However, the computationally predicted high-binder pMPPPP did not inactivate the virus to the same level, indicating that inactivation and binding are not related in the simple manner initially proposed. Nevertheless, these results indicate the potential of this tertiary amine polymer (pDEAEA) to be developed as an applied coating, for example, as materials for filtration membranes to bind and increase the efficacy toward elimination of virial contaminants in water and air.

EXPERIMENTAL PROCEDURES

Materials

All materials were used as supplied without further purification unless otherwise stated in the preparations detailed below.

Pseudo-virus particle adsorption assay

High-throughput screening was performed using a pseudo-virus adsorption assay modified from a previous study.²² Specifically, Alexa Fluor 647-tagged pseudo-virus particles were resuspended in Milli-Q water to obtain a 5 $\mu\text{g}/\text{mL}$ sample of the pseudo-virus assay solution. The array slide was washed with 20 \times 10 mL Milli-Q water and then placed immediately into 20 mL of the assay solution, incubated, and rocked in the dark gently at room temperature under ambient conditions (20°C–22°C, ~50% relative humidity [RH]) for 4 h.²² Then, the array slide was washed again with 20 \times 10 mL Milli-Q water to remove poorly attached materials. Fluorescence images of the microarray both before and after incubation were acquired using an automated wide-field fluorescence microscope (Zeiss Observer with Zeiss EC Plan 10 \times /0.5 objective, Carl Zeiss, Germany) and processed using Fiji ImageJ software (v.2017 for macOS). The border of each spot was circled to determine the material area using the composite image, which was then split into red and bright-field channels. The circle area in the red channel was used to determine the fluorescence intensity per pixel due to pseudo-virus particle binding. The autofluorescence was subtracted from the material area without the assay solution.

The Alexa Fluor 647 label was selected to enable readout fluorescence under a microscope's far-red channel, where the autofluorescence of most of the polymers in our existing library can be minimized. The concentration of pseudo-virus particles

in assay solution was optimized from 2.5 to 5 $\mu\text{g}/\text{mL}$ to give an appropriate amount of adsorption and a proper differentiation of virion adsorption abilities among spots. For the same reason, Milli-Q water was used as the resuspension medium instead of Dulbecco's buffered saline (DPBS).⁴³

Scale-up polymerization of selected monomers

2,2'-Azobis(2-methylpropionitrile) (AIBN; 1% molar ratio to monomer) was added to a solution of degassed monomers (3,360 mM) under argon. The reaction mixture was then placed immediately into a preheated 80°C oil bath and stirred overnight. The crude polymer products were purified either by precipitation or dialysis methods and then kept in a vacuum oven to remove the solvent residues or freeze dried to remove water. The obtained products were characterized by proton-nuclear magnetic resonance (¹H-NMR) and gel permeation chromatography (GPC) (Table S2; Figure S5).

Preparation of polymer-coated microslides

Polymers were dissolved in DMF solvent to achieve an approximately 4% (w/v) coating solution. 50 glass microslides (13 mm diameter) were placed into metal slide racks and activated using O₂ plasma ($p_i = 0.3$ mbar, 1,000 W, 40 kHz, 10 min). 20 μL of coating solution was added and dispersed evenly on each microslide surface. The slides were kept in a fume cupboard at room temperature overnight and then dried under vacuum in a silicone-free Heraeus vacuum oven (<0.3 mbar) for 1 week to remove volatile residues prior to use.

For MPPPP, polymer-coated slides were prepared by thermo-polymerization and coating in one step due to the limited availability of MPPPP monomers. Specifically, MPPPP monomers (3,360 mM) and AIBN initiators (1% molar ratio to monomer) were dissolved in DMF and degassed under argon. 20 μL of this solution was added and dispersed on each of the O₂ plasma-treated glass slides, which were then placed and kept on a hot plate preheated to 80°C for 3 h to complete the polymerization and coating. The slides were kept in a fume cupboard at room temperature overnight and then dried under vacuum in a silicone-free Heraeus vacuum oven (<0.3 mbar) for 1 week to remove volatile residues prior to use.

The formation of successful coatings has been confirmed by time-of-flight secondary ion mass spectrometry (ToF-SIMS) analysis from the surface distribution of the representative primary ions generated from the coating polymers (Figure S6).

Evaluation of virucidal performance

A small piece of each material (1 \times 1 cm²) was excised from the products and placed in the well of a 96-well tissue culture-treated PS plate (Corning). 10 μL of virus stock containing 7.2×10^3 TCID₅₀ of SARS-CoV-2 was added to each material piece and incubated for 10 min at room temperature and ambient humidity within a class I/III microbiological safety cabinet with the normal airflow engaged, in a containment level 3 laboratory under negative pressure. The lid of the 96-well plate was in place for the duration of the incubation. After 10 min, the surface was washed with 200 μL fresh Vero E6 cell growth medium, and the levels of SARS-CoV-2 recovered were quantified using the TCID₅₀ method.

Cellular toxicity was performed by adding Vero E6 growth medium on material surfaces of the polymers and incubated for 10 min. The medium was then added to the same TCID₅₀ assay as described above. Cell death was observed by crystal violet staining of the wells ($n = 3$) (Figure S7).

RESOURCE AVAILABILITY

Lead contact

Further information and requests for resources should be directed to and will be fulfilled by the lead contact, Xuan Xue (xuan.xue@xjtlu.edu.cn).

Materials availability

The materials generated in this study will be made available upon request.

Data and code availability

Data related to this study are provided in this article and [supplemental information](#). Additional data, related to polymer synthesis, polymer coating, pseudovirus assay, and virudical assay, are available from UoN repository: <https://doi.org/10.17639/nott.7460> or the lead contact upon reasonable request.

ACKNOWLEDGMENTS

X.X., C.M.C., J.D.D., J.K.B., C.A., and M.R.A. would like to thank the UK Research and Innovation (UK-RI) (reference no. EP/V055372/1) for funding. X.X. and C.B. would like to thank the Wellcome Trust (reference no. 204843/Z/16/Z) for funding the extension period of the project. X.X. is thankful to Research Development Funding (RDF-22-02-002) of Xi'an Jiaotong-Liverpool University for supporting the additional experiments conducted for revision. We are thankful for the Royal Society for a Wolfson Research Merit Award (WM150086) to C.A. We also thank Prof. Kin-Chow Chang, Department of Veterinary Medicine and Science, University of Nottingham, for the kind gift of Vero E6 cells.

AUTHOR CONTRIBUTIONS

M.R.A. and X.X. conceived the paper. X.X. designed and conducted the experiments, analyzed the data, wrote the original draft, and revised the manuscript. J.D.D. prepared and characterized the fluorescence tagged pseudo-virus particles and commented on the paper. C.M.C. conducted the coronavirus experiments and commented on the paper. L.C. performed machine learning regression modeling and commented on the paper. C.B. prepared the purified polymer-coated coverslips and commented on the paper. M.V.-L. conducted the additional experiments for revision. J.K.B., P.M.W., C.A., and M.R.A. discussed the results and commented on and revised the paper.

DECLARATION OF INTERESTS

The authors declare no competing interests.

SUPPLEMENTAL INFORMATION

Supplemental information can be found online at <https://doi.org/10.1016/j.xcrp.2024.102204>.

Received: August 11, 2023

Revised: July 26, 2024

Accepted: August 20, 2024

Published: September 10, 2024

REFERENCES

1. National Academies of Science, Engineering, and Medicine (2020). Rapid Expert Consultations on the COVID-19 Pandemic (The National Academies Press). <https://doi.org/10.17226/25784>.
2. Rawlinson, S., Ciric, L., and Cloutman-Green, E. (2020). COVID-19 pandemic - let's not forget surfaces. *J. Hosp. Infect.* 105, 790–791. <https://doi.org/10.1016/j.jhin.2020.05.022>.
3. Medema, G., Heijnen, L., Elsinga, G., Italiaander, R., and Brouwer, A. (2020). Presence of SARS-Coronavirus-2 RNA in Sewage and Correlation with Reported COVID-19 Prevalence in the Early Stage of the Epidemic in The Netherlands. *Environ. Sci. Technol. Lett.* 7, 511–516. <https://doi.org/10.1021/acs.estlett.0c00357>.
4. Miura, T., Okabe, S., Nakahara, Y., and Sano, D. (2015). Removal properties of human enteric viruses in a pilot-scale membrane bioreactor (MBR) process. *Water Res.* 75, 282–291. <https://doi.org/10.1016/j.watres.2015.02.046>.
5. Habibi-Yangjeh, A., Asadzadeh-Khaneghah, S., Feizpoor, S., and Rouhi, A. (2020). Review on heterogeneous photocatalytic disinfection of waterborne, airborne, and foodborne viruses: Can we win against pathogenic viruses? *J. Colloid Interface Sci.* 580, 503–514. <https://doi.org/10.1016/j.jcis.2020.07.047>.
6. Cheek, E., Guercio, V., Shrubsole, C., and Dimitroulopoulou, S. (2021). Portable air purification: Review of impacts on indoor air quality and health. *Sci. Total Environ.* 766, 142585. <https://doi.org/10.1016/j.scitotenv.2020.142585>.
7. Wu, B., Wang, R., and Fane, A.G. (2017). The roles of bacteriophages in membrane-based water and wastewater treatment processes: A review. *Water Res.* 110, 120–132. <https://doi.org/10.1016/j.watres.2016.12.004>.
8. Goswami, K.P., and Pugazhenth, G. (2020). Credibility of polymeric and ceramic membrane filtration in the removal of bacteria and virus from water: A review. *J. Environ. Manag.* 268, 110583. <https://doi.org/10.1016/j.jenvman.2020.110583>.
9. Sellaoui, L., Badawi, M., Monari, A., Tatarchuk, T., Jemli, S., Luiz Dotto, G., Bonilla-Petriciolet, A., and Chen, Z. (2021). Make it clean, make it safe: A review on virus elimination via adsorption. *Chem. Eng. J.* 412, 128682. <https://doi.org/10.1016/j.cej.2021.128682>.
10. Xue, X., Ball, J.K., Alexander, C., and Alexander, M.R. (2020). All Surfaces Are Not Equal in Contact Transmission of SARS-CoV-2.

- Matter 3, 1433–1441. <https://doi.org/10.1016/j.matt.2020.10.006>.
- Joonaki, E., Hassanpouryouzband, A., Heldt, C.L., and Areo, O. (2020). Surface Chemistry Can Unlock Drivers of Surface Stability of SARS-CoV-2 in a Variety of Environmental Conditions. *Chem* 6, 2135–2146. <https://doi.org/10.1016/j.chempr.2020.08.001>.
 - Hook, A.L., Chang, C.Y., Yang, J., Luckett, J., Cockayne, A., Atkinson, S., Mei, Y., Bayston, R., Irvine, D.J., Langer, R., et al. (2012). Combinatorial discovery of polymers resistant to bacterial attachment. *Nat. Biotechnol.* 30, 868–875. <https://doi.org/10.1038/nbt.2316>.
 - Celiz, A.D., Smith, J.G.W., Langer, R., Anderson, D.G., Winkler, D.A., Barrett, D.A., Davies, M.C., Young, L.E., Denning, C., and Alexander, M.R. (2014). Materials for stem cell factories of the future. *Nat. Mater.* 13, 570–579. <https://doi.org/10.1038/nmat3972>.
 - Patel, A.K., Celiz, A.D., Rajamohan, D., Anderson, D.G., Langer, R., Davies, M.C., Alexander, M.R., and Denning, C. (2015). A defined synthetic substrate for serum-free culture of human stem cell derived cardiomyocytes with improved functional maturity identified using combinatorial materials microarrays. *Biomaterials* 61, 257–265. <https://doi.org/10.1016/j.biomaterials.2015.05.019>.
 - Dundas, A.A., Sanni, O., Dubern, J.-F., Dimitrakis, G., Hook, A.L., Irvine, D.J., Williams, P., and Alexander, M.R. (2019). Validating a Predictive Structure–Property Relationship by Discovery of Novel Polymers which Reduce Bacterial Biofilm Formation. *Adv. Mater.* 31, 1903513. <https://doi.org/10.1002/adma.201903513>.
 - Contreas, L., Hook, A.L., Winkler, D.A., Figueredo, G., Williams, P., Loughton, C.A., Alexander, M.R., and Williams, P.M. (2023). Linear Binary Classifier to Predict Bacterial Biofilm Formation on Polyacrylates. *ACS Appl. Mater. Interfaces* 15, 14155–14163. <https://doi.org/10.1021/acsami.2c23182>.
 - Rosilo, H., McKee, J.R., Kontturi, E., Koho, T., Hytönen, V.P., Ikkala, O., and Kostianinen, M.A. (2014). Cationic polymer brush-modified cellulose nanocrystals for high-affinity virus binding. *Nanoscale* 6, 11871–11881. <https://doi.org/10.1039/C4NR03584D>.
 - Pandey, L.M. (2020). Surface engineering of personal protective equipments (PPEs) to prevent the contagious infections of SARS-CoV-2. *Surf. Eng.* 36, 901–907. <https://doi.org/10.1080/02670844.2020.1801034>.
 - Haldar, J., Chen, J., Tumpey, T.M., Gubareva, L.V., and Klibanov, A.M. (2008). Hydrophobic polycationic coatings inactivate wild-type and zanamivir- and/or oseltamivir-resistant human and avian influenza viruses. *Biotechnol. Lett.* 30, 475–479. <https://doi.org/10.1007/s10529-007-9565-5>.
 - Hsu, B.B., Yinn Wong, S., Hammond, P.T., Chen, J., and Klibanov, A.M. (2011). Mechanism of inactivation of influenza viruses by immobilized hydrophobic polycations. *Proc. Natl. Acad. Sci. USA* 108, 61–66. <https://doi.org/10.1073/pnas.1017012108>.
 - Mannelli, I., Janner, D., Sagués, F., and Reigada, R. (2017). Assessing the optimal conditions for surface-mediated disinfection of Influenza A virus solutions. *Environ. Chem.* 14, 319–326. <https://doi.org/10.1071/EN16213>.
 - Blok, A.J., Gurnani, P., Xenopoulos, A., Burroughs, L., Duncan, J., Urbanowicz, R.A., Tsoleridis, T., Müller-Kräuter, H., Strecker, T., Ball, J.K., et al. (2020). Polymer microarrays rapidly identify competitive adsorbents of virus-like particles. *Biointerphases* 15, 061005. <https://doi.org/10.1116/6.0000586>.
 - Yao, H., Song, Y., Chen, Y., Wu, N., Xu, J., Sun, C., Zhang, J., Weng, T., Zhang, Z., Wu, Z., et al. (2020). Molecular Architecture of the SARS-CoV-2 Virus. *Cell* 183, 730–738.e13. <https://doi.org/10.1016/j.cell.2020.09.018>.
 - Cai, Y., Zhang, J., Xiao, T., Peng, H., Sterling, S.M., Walsh, R.M., Jr., Rawson, S., Rits-Volloch, S., and Chen, B. (2020). Distinct conformational states of SARS-CoV-2 spike protein. *Science* 369, 1586–1592. <https://doi.org/10.1126/science.abd4251>.
 - Areo, O., Joshi, P.U., Obrenovich, M., Tayahi, M., and Heldt, C.L. (2021). Single-Particle Characterization of SARS-CoV-2 Isoelectric Point and Comparison to Variants of Interest. *Microorganisms* 9, 1606. <https://doi.org/10.3390/microorganisms9081606>.
 - Bodnarchuk, M.S., Doncom, K.E.B., Wright, D.B., Heyes, D.M., Dini, D., and O'Reilly, R.K. (2017). Polyelectrolyte pKa from experiment and molecular dynamics simulation. *RSC Adv.* 7, 20007–20014. <https://doi.org/10.1039/C6RA27785C>.
 - Yue, M., Hoshino, Y., and Miura, Y. (2015). Design rationale of thermally responsive microgel particle films that reversibly absorb large amounts of CO₂: fine tuning the pKa of ammonium ions in the particles. *Chem. Sci.* 6, 6112–6123. <https://doi.org/10.1039/C5SC01978H>.
 - Amaly, J.I., Wanless, E.J., Li, Y., Michailidou, V., Armes, S.P., and Duccini, Y. (2004). Synthesis and Characterization of Novel pH-Responsive Microgels Based on Tertiary Amine Methacrylates. *Langmuir* 20, 8992–8999. <https://doi.org/10.1021/la049156t>.
 - Zhou, K., Wang, Y., Huang, X., Luby-Phelps, K., Sumer, B.D., and Gao, J. (2011). Tunable, ultrasensitive pH-responsive nanoparticles targeting specific endocytic organelles in living cells. *Angew. Chem., Int. Ed. Engl.* 50, 6109–6114. <https://doi.org/10.1002/anie.201100884>.
 - Williams, M., Penfold, N.J.W., and Armes, S.P. (2016). Cationic and reactive primary amine-stabilised nanoparticles via RAFT aqueous dispersion polymerisation. *Polym. Chem.* 7, 384–393. <https://doi.org/10.1039/C5PY01577D>.
 - Wang, N., Ferhan, A.R., Yoon, B.K., Jackman, J.A., Cho, N.-J., and Majima, T. (2021). Chemical design principles of next-generation antiviral surface coatings. *Chem. Soc. Rev.* 50, 9741–9765. <https://doi.org/10.1039/D1CS00317H>.
 - Li, Y., Wang, Z., Wei, Q., Luo, M., Huang, G., Sumer, B.D., and Gao, J. (2016). Non-covalent interactions in controlling pH-responsive behaviors of self-assembled nanosystems. *Polym. Chem.* 7, 5949–5956. <https://doi.org/10.1039/C6PY01104G>.
 - Xie, L., Liu, F., Liu, J., and Zeng, H. (2020). A Nanomechanical Study on Deciphering the Stickiness of SARS-CoV-2 on Inanimate Surfaces. *ACS Appl. Mater. Interfaces* 12, 58360–58368. <https://doi.org/10.1021/acsami.0c16800>.
 - Weininger, D. (1988). SMILES, a chemical language and information system. 1. Introduction to methodology and encoding rules. *J. Chem. Inf. Comput. Sci.* 28, 31–36. <https://doi.org/10.1021/ci00057a005>.
 - Lovrić, M., Molero, J.M., and Kern, R. (2019). PySpark and RDKit: Moving towards Big Data in Cheminformatics. *Mol. Inform.* 38, e1800082. <https://doi.org/10.1002/minf.201800082>.
 - Landrum, G. (2016). RDKit: Open-Source Cheminformatics Software 2016_09_4. Q3 2016) Release. https://github.com/rdkit/rdkit/releases/tag/Release_2016_09_4.
 - Jost, L. (2006). Entropy and diversity. *Oikos* 113, 363–375. <https://doi.org/10.1111/j.2006.0030-1299.14714.x>.
 - Roy, K., Kar, S., and Ambure, P. (2015). On a simple approach for determining applicability domain of QSAR models. *Chemometr. Intell. Lab. Syst.* 145, 22–29. <https://doi.org/10.1016/j.chemolab.2015.04.013>.
 - Tropsha, A., and Golbraikh, A. (2007). Predictive QSAR modeling workflow, model applicability domains, and virtual screening. *Curr. Pharmaceut. Des.* 13, 3494–3504. <https://doi.org/10.2174/138161207782794257>.
 - Virustatic Shield Ltd. Virustatic shield. <https://www.virustaticshield.com/>.
 - Xue, X., Coleman, C.M., Duncan, J.D., Hook, A.L., Ball, J.K., Alexander, C., and Alexander, M.R. (2022). Evaluation of the relative potential for contact and doffing transmission of SARS-CoV-2 by a range of personal protective equipment materials. *Sci. Rep.* 12, 16654. <https://doi.org/10.1038/s41598-022-20952-8>.
 - Sorci, M., Fink, T.D., Sharma, V., Singh, S., Chen, R., Arduini, B.L., Dovidenko, K., Heldt, C.L., Palermo, E.F., and Zha, R.H. (2022). Virucidal N95 Respirator Face Masks via Ultrathin Surface-Grafted Quaternary Ammonium Polymer Coatings. *ACS Appl. Mater. Interfaces* 14, 25135–25146. <https://doi.org/10.1021/acsami.2c04165>.
 - Castaño, N., Cordts, S.C., Kurosu Jalil, M., Zhang, K.S., Koppaka, S., Bick, A.D., Paul, R., and Tang, S.K.Y. (2021). Fomite Transmission, Physicochemical Origin of Virus-Surface Interactions, and Disinfection Strategies for Enveloped Viruses with Applications to SARS-CoV-2. *ACS Omega* 6, 6509–6527. <https://doi.org/10.1021/acsomega.0c06335>.